AGU PUBLICATIONS

Geophysical Research Letters

RESEARCH LETTER

10.1002/2014GL062451

Key Points:

- Continental precipitation annual amplitude (CPAA) shows multidecadal variability
- CPAA multidecadal variability is driven by ENSO and AMO
- Recent trends in the CPAA have to be interpreted in light of this result

Supporting Information:

- Figures S1–S3

Correspondence to:
D. García-García,
d.garcia@ua.es

Citation:
García-García, D., and C. C. Ummenhofer (2015), Multidecadal variability of the continental precipitation annual amplitude driven by AMO and ENSO, *Geophys. Res. Lett.*, *42*, doi:10.1002/2014GL062451.

Received 6 NOV 2014
Accepted 31 DEC 2014
Accepted article online 8 JAN 2015

Multidecadal variability of the continental precipitation annual amplitude driven by AMO and ENSO

David García-García[1] and Caroline C. Ummenhofer[2]

[1]Department of Applied Mathematics, EPS, University of Alicante, San Vicente del Raspeig, Spain, [2]Department of Physical Oceanography, Woods Hole Oceanographic Institution, Woods Hole, Massachusetts, USA

Abstract As the water vapor content in the atmosphere scales with temperature, a warmer world is expected to feature an intensification of the hydrological cycle. Work to date has mainly focused on mean precipitation changes, whose connection to climatic modes is elusive at a global scale. Here we show that continental precipitation annual amplitude, which represents the annual range between minimum and maximum (monthly) rainfall, covaries with a linear combination of the Atlantic Multidecadal Oscillation and low-frequency variations in the El Niño–Southern Oscillation on a decadal to multidecadal scale with a correlation coefficient of 0.92 ($P < 0.01$). The teleconnection is a result of changes in moisture transport in key regions. Reported trends in the annual amplitude of global precipitation in recent decades need to be assessed in light of this substantial low-frequency variability, which could mask or enhance an anthropogenic signal in hydrological cycle changes.

1. Introduction

Changes in the hydrological cycle have the potential to affect a large proportion of the world's population through impacts on available water resources. In a warming world, expected future precipitation changes that follow a "rich gets richer" pattern to first-order result from the thermodynamic effect of moisture changes in the atmosphere [*Chou and Neelin*, 2004; *Held and Soden*, 2006]. Warmer temperatures increase atmospheric global mean water vapor content, which will lead to enhanced precipitation over climatological wet regions due to low-level moisture convergence under a constant relative humidity constraint [*Held and Soden*, 2006]. In the last 40 years, global water vapor and temperature have increased by 3.5% and 0.5°C, respectively. Both are expected to continue to rise in the 21st century [*Hartmann et al.*, 2013], resulting in an intensification of the hydrological cycle [*Held and Soden*, 2006; *Huntington*, 2006; *Wentz et al.*, 2007; *Chou et al.*, 2013; *Hartmann et al.*, 2013]. Under such a scenario, the climatologically wet regions in the tropics and midlatitude storm tracks are expected to receive enhanced precipitation, while the dry descending regions of the meridional Hadley circulation in the subtropics will be subjected to drier conditions. Nevertheless, the precipitation changes seem to be more complicated as this description works over the ocean, while it may be an oversimplification over land where only 10.8% of its area follows the "dry gets drier, wet gets wetter" pattern [*Greve et al.*, 2014].

Beyond the annual total precipitation amount, global and regional precipitation is defined by the distribution through the year, which is a crucial aspect of societal and ecological importance. Changes in the redistribution of rainfall from dry to wet seasons could increase the risk of hydroclimatic extremes, such as drought and flooding. Recently, *Chou et al.* [2013] reported that the difference in precipitation between wet and dry seasons has been increasing over recent decades and is expected to continue in the 21st century [*Collins et al.*, 2013]. However, understanding multidecadal changes in that precipitation amplitude is important to interpret those results. Here we describe such multidecadal variability at a global scale over the past century and analyze its connection with two leading modes of variability: El Niño–Southern Oscillation (ENSO) and Atlantic Multidecadal Oscillation (AMO). They are characterized by recurrent, substantial anomalies in the ocean-atmosphere system in the Pacific and Atlantic Oceans, respectively, and are associated with large-scale reorganization of the atmospheric circulation and precipitation changes around the globe [e.g., *Ropelewski and Halpert*, 1987; *Knight et al.*, 2006]. Rather than focus on the mechanisms by which ENSO and AMO influence regional precipitation patterns, we assess their relationship with the range of the seasonal cycle of global precipitation on multidecadal time scales.

2. Seasonal Cycle of Continental Precipitation

We use global monthly gridded precipitation data over land based on quality-controlled rain gauges from Global Precipitation Climatology Centre version 6 (GPCCv6) [*Schneider et al*., 2011], although results are robust across different precipitation products (for details, see below and Figure 2b). The seasonal cycle of precipitation is revealed through a complex empirical orthogonal function (CEOF) [*Preisendorfer*, 1988] analysis applied to the centered and not detrended time series for the period of 1901–2010. The first CEOF mode (Figure 1) explains 63% of the total variance and corresponds to an annual signal, since Figure 1d shows a straight line decreasing 360°/yr, which means a complete cycle per year. The annual amplitude shows the strongest signal in the monsoonally dominated regions in Southeast Asia, India, the Maritime Continent, much of Africa, and South and Central America and weakest signal in the desert regions of the Sahara, Arabian Peninsula, central Asia, central Australia, and western U.S. (Figure 1a). The high-precipitation regions near the equator exhibit low annual amplitude because the precipitation is uniformly distributed throughout the year. This pattern differs notably from the *mean* precipitation (Figure 1a versus Figure S1 in the supporting information). The annual maximum of precipitation is spatially dependent, with a difference of ~6 months between the Northern and Southern Hemispheres (Figure 1b). The former reaches the annual maximum in boreal summer (with some exceptions around the Mediterranean Sea, Southeast Asia, and some regions in North America), while the latter reaches it in boreal winter. Hereafter, when a season is mentioned for a region, it will refer to the corresponding boreal or austral season for the respective hemisphere.

The continental precipitation annual amplitude (CPAA), which represents the variability of the global difference between wet and dry seasons over land, varies over time (Figure 1c). It exhibits decadal to multidecadal variability as highlighted by the 13 year running mean, with above-average values during the period of 1920–1960 and below-average values during 1970–2000. As this signal is the object of this study, we verified that it is not an artifact of the CEOF. The CPAA is estimated with an alternative approach: for each grid point, the annual amplitude is estimated in a 13 year moving window by least squares fitting and assigned to the center of the window. This approach allows us to average the annual amplitude for any grid point. When globally averaged, the resultant time series has a correlation with the annual amplitude from the first CEOF mode of 0.97 (Figure 2a), significant at a 99% level of confidence. Due to the high degree of serial correlation in the smoothed time series, the significance level is estimated according to a specific Monte Carlo analysis based on the randomization of phases in the frequency domain ([*Ebisuzaki*, 1997] note that this methodology is applied for all the correlations estimated in the manuscript). Therefore, different approaches show the same decadal to multidecadal variability.

In addition to the GPCCv6 data set, the analyses were also repeated with additional rainfall products. These include Climatic Research Unit (CRU) v3.1 (1901–2012 [*Matsuura and Willmott*, 2012]), University of Delaware Air Temperature and Precipitation (UDel_AirT_Precip) v3.01 (1900–2010), NOAA's PRECipitation REConstruction over Land (NOAA PREC/L) (1948–2013 [*Chen et al*., 2002]), and Climate Prediction Center Merged Analysis of Precipitation (CMAP) (1979–2011 [*Xie and Arkin*, 1997]). All of them show the same low-frequency signal, which is in good agreement during the common periods, especially in the second half of the twentieth century, when the number of observations is higher (Figures 2b and 2c).

3. ENSO and AMO Teleconnections

Leading modes of climate variability exert substantial impact on regional mean precipitation around the world, but do they contribute to the observed multidecadal variations in the CPAA?

ENSO is the leading mode of interannual variability, with a dominant period of 3–7 years, and associated with large-scale reorganization of the ocean-atmosphere system in the Pacific Ocean and surrounding regions. The Southern Oscillation Index (SOI), as the monthly atmospheric pressure difference between Tahiti and Darwin, Australia, estimated by the Australian Bureau of Meteorology is used here (ftp://ftp.bom.gov.au/anon/home/ncc/www/sco/soi/soiplaintext.html). To focus on the low-frequency component of ENSO, the SOI is smoothed with a 13 year moving window. The warm phase of ENSO, El Niño, is associated with negative values of the SOI: A decrease in the pressure difference between the eastern and western Pacific results in a weakening or reversal of the climatological easterlies over the equatorial Pacific, along with a relaxation of the thermocline gradient, and associated warming of the central and eastern Pacific sea surface temperature (SST).

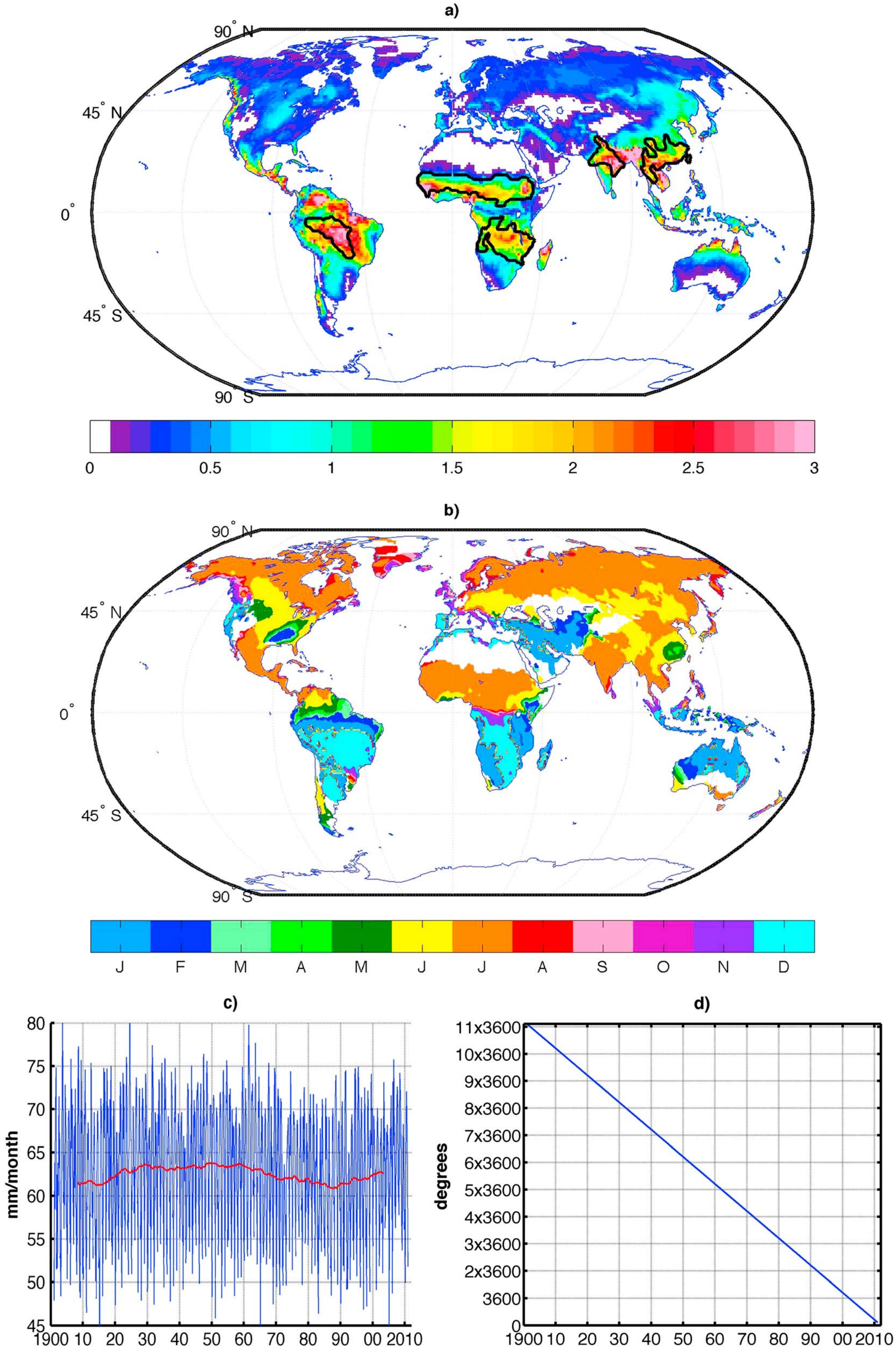

Figure 1. First CEOF of precipitation data accounting for 63% of the variance. (a) Amplitude of the complex spatial pattern (the white regions mean no variability in this mode), (b) phase of the complex spatial pattern, (c) amplitude of the complex expansion coefficient (the red line is a smoothing of the signal with a 13 year moving window), and (d) phase of the complex expansion coefficient. Selected regions highlighted with black thick contours in Figure 1a represent a time-average annual amplitude larger than 60 mm/yr, the so-called high-amplitude regions.

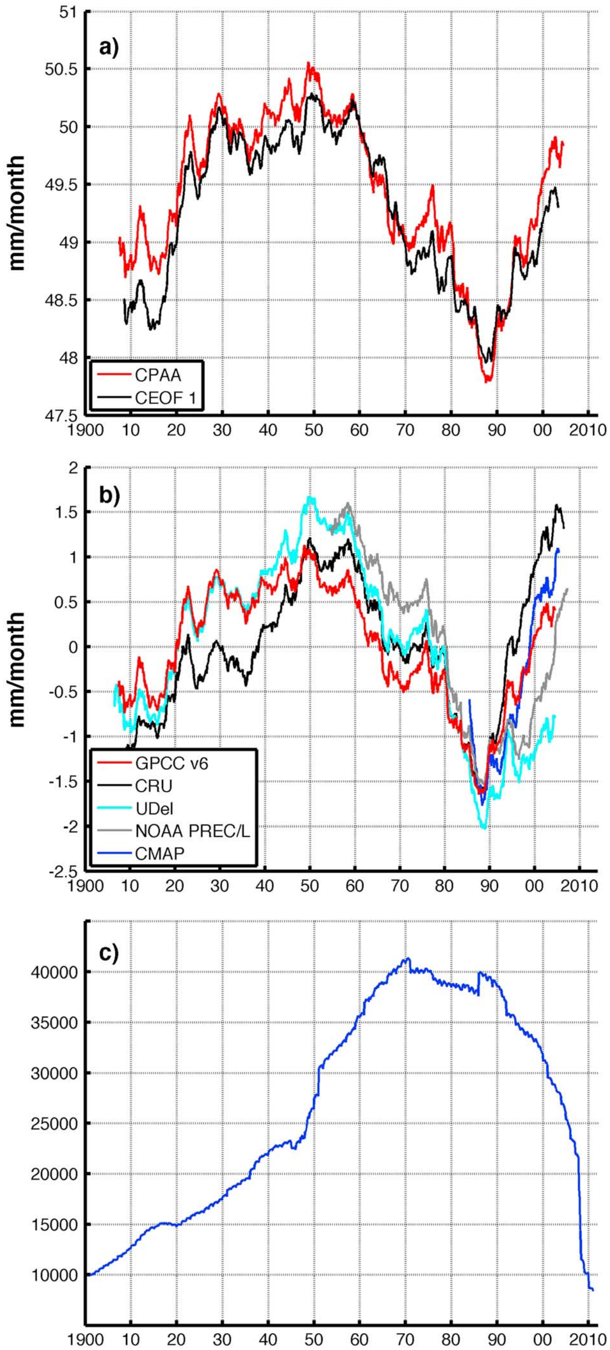

Figure 2. CPAA for different data sets, all smoothed with a 13 year moving window. (a) The red line shows GPCCv6 data set (1901–2010). The black line is the amplitude of the CEOF1 time series. (b) CPAA estimated from different data sets as indicated. (c) Number of observations for GPCCv6.

El Niño events are associated with above-average rainfall in the southwestern and southeastern U.S., southeastern South and Central America and anomalous dry conditions in India, the Maritime Continent, and eastern Australia [e.g., *Ropelewski and Halpert*, 1987] and droughts more broadly in the tropics [*Lyon*, 2004].

The AMO monthly time series is estimated as the detrended area-weighted average over the North Atlantic (from the equator to 70°N) based on the Kaplan Extended SST v2 [*Kaplan et al*., 1998], and it is provided by NOAA/Office of Oceanic and Atmospheric Research/Earth System Research Laboratory Physical Sciences Division (NOAA/OAR/ESRL PSD) (http://www.esrl.noaa.gov/psd/data/correlation/amon.us.long.data). The AMO exhibits a period of around 60–80 years [*Enfield et al*., 2001; *Deser et al*., 2010]. A warm phase of the AMO occurred in the period of approximately 1920–1960, while the North Atlantic was unusually cold during the period of 1970–1990. Warm/cold AMO phases have been linked to variations in the strength of the thermohaline circulation in the North Atlantic [e.g., *Knight et al*., 2005; *Gastineau and Frankignoul*, 2012] or emerging from ocean-atmosphere coupling [e.g., *Frankignoul et al*., 1997; *Häkkinen et al*., 2011]. The positive phase of the AMO has been related to the above-average rainfall in western Europe [*Sutton and Hodson*, 2005], the Sahel [*Folland et al*., 1986; *Knight et al*., 2006; *Zhang and Delworth*, 2006; *Ting et al*., 2009], India [*Goswami et al*., 2006; *Zhang and Delworth*, 2006], and Southeast Asia [*Lu et al*., 2006] and with the below-average precipitation in the U.S. [*Enfield et al*., 2001; *Sutton and Hodson*, 2005] and northeast Brazil [*Knight et al*., 2006; *Zhang and Delworth*, 2006].

Rainfall variability in many regions across the globe is influenced by the phases of ENSO and the AMO. But how do they relate to the decadal to multidecadal variability in the CPAA? For this, a linear regression of the CPAA against the combination $a \times \mathrm{SOI} + b \times \mathrm{AMO}$ is estimated. The coefficients $a = 0.57 \pm 0.03$ and $b = 0.61 \pm 0.03$ present the minimal residual with a correlation of 0.92 ($P < 0.01$; Figure 3a). Note that this analysis is qualitatively robust to the use of the specific ENSO index (see Figure S2 in the supporting information for Niño 1 + 2, Niño 3, Niño 4, and Niño 3.4). The SOI and AMO coefficients are of similar magnitude, indicating that ENSO and AMO modulate the CPAA in equal measure. However, is this statistical relationship based on any physical connection? To elucidate this question, two

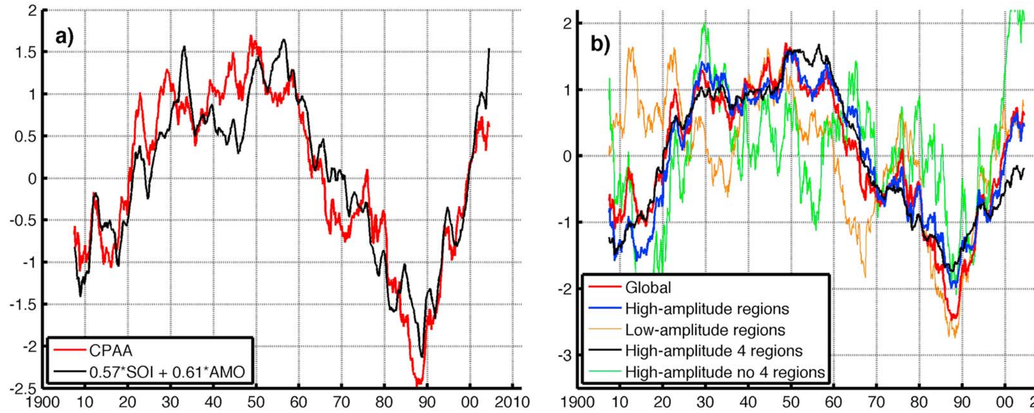

Figure 3. Time series of the amplitude of precipitation globally and regionally and for ENSO and AMO. (a) The red line is the global CPAA estimated in 13 year moving windows. The black line is $0.57 \times \text{SOI} + 0.61 \times \text{AMO}$. SOI and AMO are smoothed with 13 year running windows. (b) Precipitation annual amplitude averaged in several regions as defined in the text: global (red line), high-amplitude regions (blue line), low-amplitude regions (orange line), four subregions selected among the high-amplitude regions (black line), and high-amplitude regions not selected (green line). All time series are centered on 0 and normalized to 1 standard deviation.

keypoints must be addressed: (1) Are regions equally important when studying the CPAA? (2) Is the CPAA related to the global mean precipitation?

First, the signal in regions with annual amplitude above 60 mm/yr (with values >1 in Figure 1a, hereafter denoted as "high-amplitude regions") is highly correlated ($R = 0.95$, $P < 0.01$) with the CPAA (Figure 3b). On the contrary, the correlation between the CPAA and the regions with annual amplitude below 60 mm/yr ("low-amplitude regions") decreases to 0.71 ($P < 0.03$; Figure 3b). Furthermore, not all the high-amplitude regions follow the same decadal to multidecadal variability, as can be deduced from the map of correlation coefficients between the grid points and the CPAA (Figure S3 in the supporting information). Four regions with uniform high correlation appear among the high-amplitude regions: (1) Brazilian southern Amazon basin (confined to the Southern Hemisphere), (2) Sahel, (3) southern Africa, and (4) north India and southeastern Asia (contoured regions in Figure 1a). The signal averaged over these four regions has a correlation of 0.94 ($P < 0.01$) with the CPAA, while the correlation of the remaining high-amplitude regions decreases to 0.57 ($P < 0.01$; Figure 3b). Therefore, we focus our analysis on the influence of ENSO and AMO on the CPAA in these four high-amplitude regions, which represent 10% of the continental surface with precipitation data, 16% of the total precipitation, and 23% of the total annual amplitude signal.

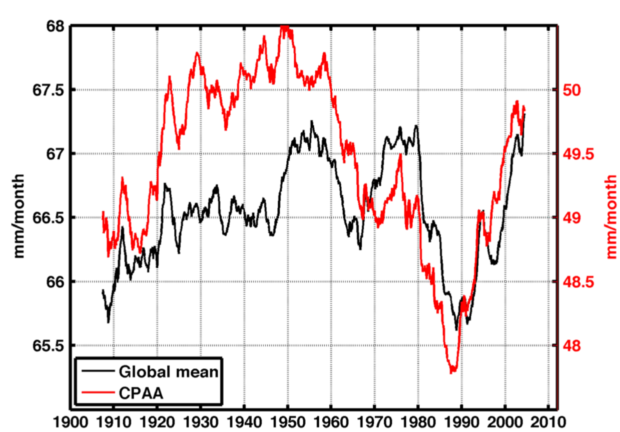

Figure 4. The red line is the CPAA estimated in 13 year moving windows as in Figure 3a, and the black line is the continental mean precipitation.

Second, the multidecadal variability in the CPAA differs from that in the global mean precipitation (Figure 4). The two time series are correlated at only 0.59 ($P > 0.1$). Differences arise when the variability of the precipitation differs from one season to another. For example, consider a region which reaches its annual maximum and minimum in summer and winter, respectively. Then, an increase of summer precipitation would increase the annual amplitude, while an increase in winter precipitation would decrease it. However, the annual mean precipitation would increase in both cases. For that reason, this study needs to incorporate seasonal rainfall distributions. As both coefficients of the

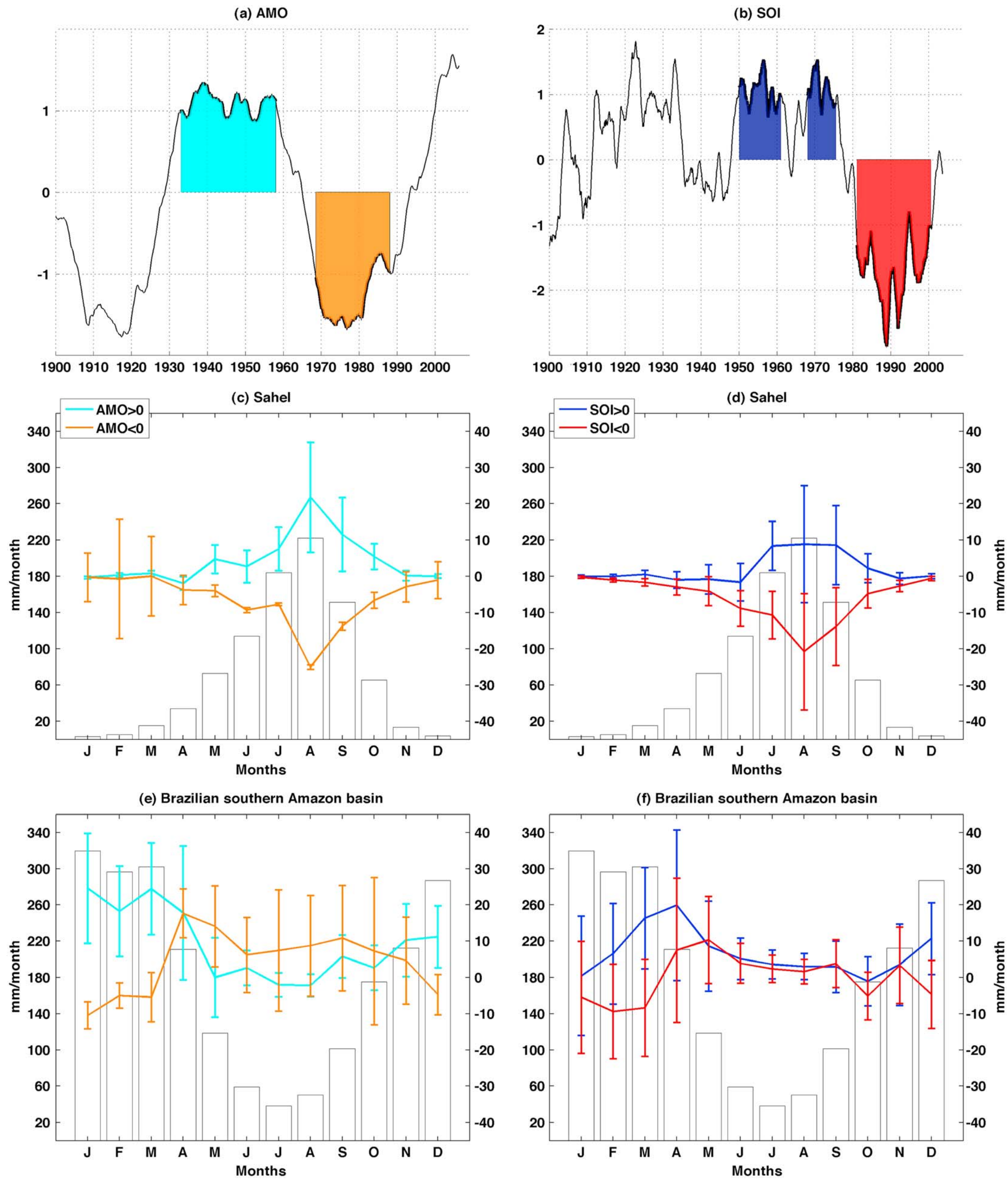

Figure 5. (a) AMO index and (b) SOI. The colored periods correspond to the selected positive and negative phases of AMO (positive: 1933–1957 and negative: 1968.5–1987) and SOI (positive: 1950–1960 and 1968–1975.5 and negative: 1981–2000.5). Both curves are smoothed with a 13 year moving window, centered on zero, and normalized to 1 standard deviation. The bars represent the mean annual cycle for (c and d) Sahel, (e and f) Brazilian southern Amazon basin, (g and h) southern Africa, and (i and j) India and southeastern Asia. The values are indicated on the left-hand *y* axis. The colored lines represent the deviations from the annual cycles (cf., right-hand *y* axis) for the periods described in Figures 5a and 5b: positive SOI (blue line), negative SOI (red line), positive AMO (cyan line), and negative AMO (orange line). The error bars are the standard deviations for each month estimated from 1000 random length-period sections of the time series, whose lengths match that from the respective period, according to *Ebisuzaki* [1997].

linear regression are positive, both SOI and AMO should be positively correlated with the CPAA; i.e., positive phases of the SOI and AMO should produce above-average annual amplitudes, which could be reached with above-average precipitation in the season of maximum precipitation, or with below-average precipitation in the season of minimum precipitation.

Key positive (negative) phases of multidecadal variability in the ENSO and AMO time series (Figures 5a and 5b) are selected as follows: starting with the January or July after the index time series first exceeds 1 standard deviation from the mean until the last June or December after the index changes sign to a negative (positive)

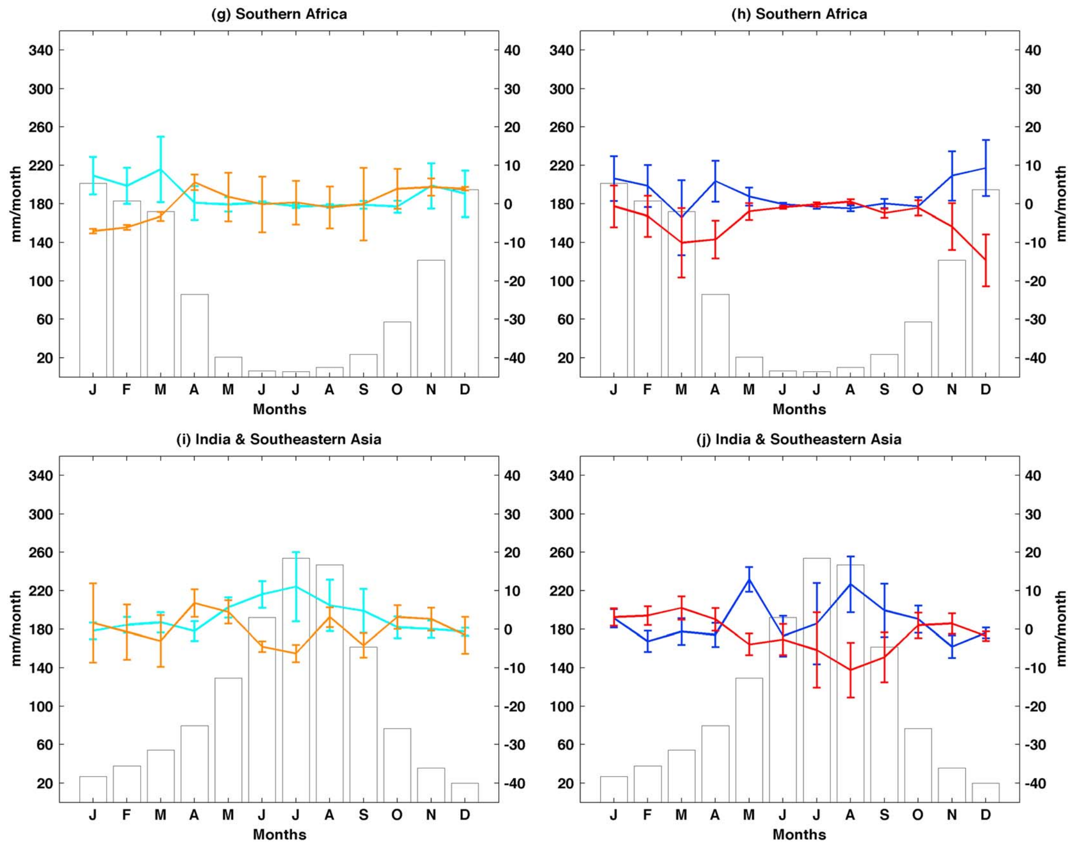

Figure 5. (continued)

phase. The period prior to 1930 is disregarded as it is expected to be less accurate because of the lower number of observations (Figure 2c).

The mean annual cycle of the selected four high-amplitude subregions and their corresponding anomalies during positive and negative phases of AMO and low-frequency component of ENSO is shown in Figure 5. In the Sahel, the annual precipitation maximum is reached in summer, and it is increased (decreased) during the positive (negative) phases of AMO and SOI (Figures 5c and 5d). The positive (negative) AMO is associated with a northward (southward) shift of the Intertropical Convergence Zone (ITCZ), which produces above-average (below-average) summer rainfall in the Sahel and India [*Knight et al.*, 2006; *Zhang and Delworth*, 2006]. The analysis of the error bars (estimated as the standard deviation derived from a Monte Carlo method according to *Ebisuzaki* [1997]) suggests that the influence of AMO is more robust than ENSO, as shown previously on interannual time scales [*Ward*, 1998; *Giannini et al.*, 2003].

Warm (cool) SST in the tropical Atlantic results in a reduction (increase) of moisture transport from the Atlantic to the Amazon basin during the winter, diminishing (enhancing) rainfall during the dry season, and decreasing (increasing) the annual minimum [*Ronchail et al.*, 2002; *Yoon and Zeng*, 2010]. In 2005, this mechanism produced a severe drought in the Amazon [*Zeng et al.*, 2008; *Marengo et al.*, 2008]. However, this feature is not observed in the anomaly annual cycle for the southern Amazon basin, at least within the error estimate (Figure 5e). Instead, a positive precipitation anomaly in summer during the positive phase of the AMO is seen, which to our knowledge has not been reported in the literature. Negative AMO produces the opposite scenario. Regarding ENSO, the positive (negative) phase of SOI increases (decreases) the rainfall in the Amazon basin during summer, increasing (decreasing) the annual maximum [*Ropelewski and Halpert*, 1987; *Ronchail et al.*, 2002; *Yoon and Zeng*, 2010]. Both AMO and ENSO affect the precipitation in the Amazon basin, as has been exploited in recent fire forecast models [*Chen et al.*, 2011; *Fernandes et al.*, 2011].

In southern Africa, the rainy season is in summer, and its intensity is driven by moisture transport from both Atlantic and Indian Oceans [*Rouault et al.*, 2003; *Giannini et al.*, 2008; *Jury*, 2013]. Warm SST in the tropical southeastern Atlantic is associated with the above-average rainfall along the Angolan and Namibian coast during late summer, which also affects inland regions when the moisture transport from the Indian Ocean is greater than average [*Rouault et al*., 2003]. Positive AMO also acts to warm tropical southeast Atlantic SST and thus to enhance the annual maximum rainfall. However, the ITCZ moves northward during that AMO phase, which reduces summer precipitation [*Jury*, 2013]. Although these opposite consequences are not yet resolved [*Jury*, 2013], our results suggest that the positive AMO enhances South African summer rainfall (Figure 5g). The positive SOI is also associated with above-average summer rainfall [*Ropelewski and Halpert*, 1987; *Nicholson and Kim*, 1997; *Giannini et al*., 2008]. During the negative phases of both AMO and SOI, the opposite is true.

In India and southeastern Asia, the positive (negative) phase of the AMO is associated with above-normal (below-normal) summer and autumn rainfall (Figure 5i) [*Goswami et al*., 2006; *Lu et al*., 2006]. On the other hand, positive (negative) SOI enhances (weakens) rainfall during the summer monsoon [*Ropelewski and Halpert*, 1987; *Goswami et al*., 2006] (Figure 5j). Then, positive (negative) phases of both AMO and SOI increase (decrease) the annual maximum in the region.

In summary, Figures 5c–5j support the idea that both AMO and ENSO are positively correlated with the annual precipitation amplitude in the four regions selected and by inference then with the CPAA.

4. Discussion

The AMO and ENSO time series used here exhibit low correlation ($R = 0.01$, $P = 0.98$), echoing results by *de Viron et al*. [2013]. Despite this, they are not completely independent entities. The positive phase of the AMO is associated with anomalous easterly winds over the central and western equatorial Pacific that deepen the thermocline in the west Pacific, reducing ENSO variability [*Dong et al*., 2006; *Dong and Sutton*, 2007; *Timmermann et al*., 2007; *Kang et al*., 2014]. AMO thus modulates ENSO characteristics and by inference its impacts. For example, El Niño-related rainfall increases (decreases) during the negative (positive) phases of the AMO in Florida [*Goly and Teegavarapu*, 2014] and South America [*Kayano and Capistrano*, 2014]. Conversely, ENSO also modulates the AMO-related summer rainfall in North America [*Hu and Feng*, 2012]. Furthermore, the Pacific Decadal Oscillation, which is known to be associated with low-frequency ENSO variability and modulates the relationship between ENSO and the global climate [*Wang et al*., 2014], may be related to the AMO [*d'Orgeville and Peltier*, 2007]. Irrespective of the relationship between ENSO and AMO, their combination shows a robust connection with the multidecadal variability of the CPAA. On the other hand, other modes of variability, such as the Pacific Decadal Oscillation and the North Atlantic Oscillation, do not exhibit strong relationships to the CPAA on multidecadal time scales.

CPAA shows a decadal to multidecadal oscillation with a period of 70–80 years, although the span of precipitation data is too short to ensure that it has been a sustained oscillation in the past or how it will behave in the future. Low-frequency variability of global precipitation can be connected to two of the most important climatic modes, AMO and ENSO, through annual amplitude variability. Understanding this relationship would help to predict future changes of the precipitation distribution through the year. Furthermore, the reported oscillation should be taken into account when interpreting the enhancement of the range of the precipitation observed in the last three decades [*Chou et al*., 2013].

Acknowledgments
We gratefully acknowledge the groups producing and making their data sets available and the agencies providing them. The SOI has been provided by the Australian Bureau of Meteorology, the oceanic ENSO indices by NOAA/NWS/CPC, and the AMO index by NOAA/OAR/ESRL PSD. The use of the following precipitation data sets is gratefully acknowledged: Global Precipitation Climatology Centre by the German Weather Service (DWD) accessed through http://gpcc.dwd.de; Climatic Research Unit by the University of East Anglia, UK; and University of Delaware Air Temperature and Precipitation, NOAA's PRECipitation RECOnstruction over Land, and CPC Merged Analysis of Precipitation provided through the NOAA/OAR/ESRL PSD website. The following observational/reanalysis products also informed our analysis: Hadley Centre HadISST by the UK Met Office, and the Twentieth Century Reanalysis Project supported by the U.S. DOE, Office of Science Innovative and Novel Computational Impact on Theory and Experiment program, and Office of Biological and Environmental Research, and by the NOAA Climate Program Office. D.G.G. was supported through a Spanish Project (CGL2010-12153-E) and the Generalitat Valenciana (GV/2013/144 and ACOMP-2013-068) and C.C.U. through the *Penzance* and *John P. Chase Memorial Endowed Funds* at WHOI.

The Editor thanks Alessandra Giannini and an anonymous reviewer for their assistance in evaluating this paper.

References

Chen, M., P. Xie, J. E. Janowiak, and P. A. Arkin (2002), Global land precipitation: A 50 year monthly analysis based on gauge observations, *J. Hydrometeorol.*, *3*, 249–266.

Chen, Y., J. T. Randerson, D. C. Morton, R. S. DeFries, G. J. Collatz, P. S. Kasibhatla, L. Giglio, Y. Jin, and M. E. Marlier (2011), Forecasting fire season severity in South America using sea surface temperature anomalies, *Science*, *334*, 787–791.

Chou, C., and J. D. Neelin (2004), Mechanisms of global warming impacts on regional tropical precipitation, *J. Clim.*, *17*, 2688–2701.

Chou, C., J. C. H. Chiang, C.-W. Lan, C.-H. Chung, Y.-C. Liao, and C.-J. Lee (2013), Increase in the range between wet and dry season precipitation, *Nat. Geosci.*, *6*, 263–267, doi:10.1038/NGEO1744.

Collins, M., et al. (2013), Long-Term Climate Change: Projections, Commitments, and Irreversibility, in *Climate Change 2013: The Physical Science Basis. Contribution of Working Group I to the Fifth Assessment Report of the Intergovernmental Panel on Climate Change*, edited by T. F. Stocker, pp. 1029–1136, Cambridge Univ. Press, Cambridge, U. K., and New York.

Deser, C., M. A. Alexander, S.-P. Xie, and A. S. Phillips (2010), Sea surface temperature variability: Patterns and mechanisms, *Annu. Rev. Mar. Sci.*, *2*, 115–143.

de Viron, O., J. O. Dickey, and M. Ghil (2013), Global modes of climate variability, *Geophys. Res. Lett.*, *40*, 1832–1837, doi:10.1002/grl.50386.

Dong, B., and R. T. Sutton (2007), Enhancement of ENSO variability by a weakened Atlantic thermohaline circulation in a coupled GCM, *J. Clim.*, *20*, 4920–4939, doi:10.1175/JCLI4284.1.

Dong, B., R. T. Sutton, and A. A. Scaife (2006), Multidecadal modulation of El Niño–Southern Oscillation (ENSO) variance by Atlantic Ocean sea surface temperatures, *Geophys. Res. Lett.*, *33*, L08705, doi:10.1029/2006GL025766.

d'Orgeville, M., and W. R. Peltier (2007), On the Pacific Decadal Oscillation and the Atlantic Multidecadal Oscillation: Might they be related?, *Geophys. Res. Lett.*, *34*, L23705, doi:10.1029/2007GL031584.

Ebisuzaki, W. (1997), A method to estimate the statistical significance of a correlation when the data are serially correlated, *J. Clim.*, *10*, 2147–2153.

Enfield, D. B., A. M. Mestas-Nuñez, and P. Trimble (2001), The Atlantic Multidecadal Oscillation and its relation to rainfall and river flows in the continental U.S., *Geophys. Res. Lett.*, *28*, 2077–2080, doi:10.1029/2000GL012745.

Fernandes, K., W. Baethgen, S. Bernardes, R. DeFries, D. G. DeWitt, L. Goddard, W. Lavado, D. E. Lee, C. P. M. Pinedo-Vasquez, and M. Uriarte (2011), North Tropical Atlantic influence on western Amazon fire season variability, *Geophys. Res. Lett.*, *38*, L12701, doi:10.1029/2011GL047392.

Folland, C. K., T. N. Palmer, and D. E. Parker (1986), Sahel rainfall and worldwide sea temperatures, 1901–85, *Nature*, *320*, 602–607, doi:10.1038/320602a0.

Frankignoul, C., P. Muller, and E. Zorita (1997), A simple model of the decadal response of the ocean to stochastic wind forcing, *J. Phys. Oceanogr.*, *27*, 1533–1546.

Gastineau, G., and C. Frankignoul (2012), Cold-season atmospheric response to the natural variability of the Atlantic meridional overturning circulation, *Clim. Dyn.*, *39*, 37–57.

Giannini, A., R. Saravanan, and P. Chang (2003), Oceanic forcing of Sahel rainfall on interannual to interdecadal time scales, *Science*, *302*, 1027–1030, doi:10.1126/science.1089357.

Giannini, A., M. Biasutti, I. M. Held, and A. H. Sobel (2008), A global perspective on African climate, *Clim. Change*, *90*, 359–383, doi:10.1007/s10584-008-9396-y.

Goly, A., and R. S. V. Teegavarapu (2014), Individual and coupled influences of AMO and ENSO on regional precipitation characteristics and extremes, *Water Resour. Res.*, *50*, 4686–4709, doi:10.1002/2013WR014540.

Goswami, B. N., M. S. Madhusoodanan, C. P. Neema, and D. Sengupta (2006), A physical mechanism for North Atlantic SST influence on the Indian summer monsoon, *Geophys. Res. Lett.*, *33*, L02706, doi:10.1029/2005GL024803.

Greve, P., B. Orlowsky, B. Mueller, J. Sheffield, M. Reichstein, and S. I. Seneviratne (2014), Global assessment of trends in wetting and drying over land, *Nat. Geosci.*, *7*, 716–721, doi:10.1038/ngeo2247.

Häkkinen, S., P. B. Rhines, and D. L. Worthen (2011), Atmospheric blocking and Atlantic multidecadal ocean variability, *Science*, *334*, 655–659.

Hartmann, D. L., et al. (2013), Observations: Atmosphere and Surface, in *Climate Change 2013: The Physical Science Basis. Contribution of Working Group I to the Fifth Assessment Report of the Intergovernmental Panel on Climate Change*, edited by T. F. Stocker, pp. 159–254, Cambridge Univ. Press, Cambridge, U. K., and New York.

Held, I. M., and B. J. Soden (2006), Robust responses of the hydrological cycle to global warming, *J. Clim.*, *19*, 5686–5699.

Hu, Q., and S. Feng (2012), AMO- and ENSO-driven summertime circulation and precipitation variations in North America, *J. Clim.*, *25*, 6477–6495, doi:10.1175/JCLI-D-11-00520.1.

Huntington, T. G. (2006), Evidence for intensification of the global water cycle: Review and synthesis, *J. Hydrol.*, *319*, 83–95, doi:10.1016/j.jhydrol.2005.07.003.

Jury, M. R. (2013), A return to wet conditions over Africa: 1995–2010, *Theor. Appl. Climatol.*, *111*, 471–481, doi:10.1007/s00704-012-0677-z.

Kang, I., H. No, and F. Kucharski (2014), ENSO amplitude modulation associated with the mean SST changes in the tropical central Pacific induced by Atlantic Multidecadal Oscillation, *J. Clim.*, *27*, 7911–7920, doi:10.1175/JCLI-D-14-00018.1.

Kaplan, A., M. Cane, Y. Kushnir, A. Clement, M. Blumenthal, and B. Rajagopalan (1998), Analyses of global sea surface temperature 1856–1991, *J. Geophys. Res.*, *103*, 18,567–18,589, doi:10.1029/97JC01736.

Kayano, M. T., and V. B. Capistrano (2014), How the Atlantic Multidecadal Oscillation (AMO) modifies the ENSO influence on the South American rainfall, *Int. J. Climatol.*, *34*, 162–178.

Knight, J., R. J. Allan, C. K. Folland, M. Vellinga, and M. E. Mann (2005), A signature of persistent natural thermohaline circulation cycles in observed climate, *Geophys. Res. Lett.*, *32*, L20708, doi:10.1029/1005GL024233.

Knight, J. R., C. K. Folland, and A. A. Scaife (2006), Climate impacts of the Atlantic Multidecadal Oscillation, *Geophys. Res. Lett.*, *33*, L17706, doi:10.1029/2006GL026242.

Lu, R., B. Dong, and H. Ding (2006), Impact of the Atlantic Multidecadal Oscillation on the Asian summer monsoon, *Geophys. Res. Lett.*, *33*, L24701, doi:10.1029/2006GL027655.

Lyon, B. (2004), The strength of El Niño and the spatial extent of tropical drought, *Geophys. Res. Lett.*, *31*, L21204, doi:10.1029/2004GL020901.

Marengo, J. A., C. A. Nobre, J. Tomasella, M. D. Oyama, G. S. De Oliveira, R. De Oliveira, H. Camargo, L. M. Alves, and I. F. Brown (2008), The drought of Amazonia in 2005, *J. Clim.*, *21*(3), 495–516, doi:10.1175/2007JCLI1600.1.

Matsuura, K., and C. J. Willmott (2012), Terrestrial Precipitation: 1900–2010 Gridded Monthly Time Series (Version 3.02). [Available at http://climate.geog.udel.edu/~climate/html_pages/Global2011/Precip_revised_3.02/README.GlobalTsP2011.html.]

Nicholson, S. E., and J. Kim (1997), The relationship of the El Niño–Southern Oscillation to African rainfall, *Int. J. Climatol.*, *17*, 117–135.

Preisendorfer, R. W. (1988), *Principal Component Analysis in Meteorology and Oceanography*, Elsevier Sci., New York.

Ronchail, J., G. Cochonneau, M. Molinier, J. L. Guyot, A. G. D. Chaves, V. Guimaraes, and E. de Oliveira (2002), Interannual rainfall variability in the Amazon basin and sea-surface temperatures in the equatorial Pacific and the tropical Atlantic Oceans, *Int. J. Climatol.*, *22*, 1663–1686.

Ropelewski, C. F., and M. S. Halpert (1987), Global and regional precipitation patterns associated with El Niño–Southern Oscillation, *Mon. Weather Rev.*, *115*, 1606–1625.

Rouault, M., P. Florenchie, N. Fauchereau, and C. J. C. Reason (2003), Southeast tropical Atlantic warm events and southern African rainfall, *Geophys. Res. Lett.*, *30*(5), 8009, doi:10.1029/2002GL014840.

Schneider, U., A. Becker, P. Finger, A. Meyer-Christoffer, B. Rudolf, and M. Ziese, (2011), GPCC Full Data Reanalysis Version 6.0 at 1.0°: Monthly Land-Surface Precipitation from Rain-Gauges built on GTS-based and Historic Data, doi:10.5676/DWD_GPCC/FD_M_V6_100.

Sutton, R. T., and D. L. R. Hodson (2005), Atlantic Ocean forcing of North American and European summer climate, *Science*, *309*, 115–118.

Timmermann, A., et al. (2007), The influence of a weakening of the Atlantic meridional overturning circulation on ENSO, *J. Clim.*, *20*, 4899–4919, doi:10.1175/JCLI4283.1.

Ting, M., Y. Kushnir, R. Seagar, and C. Li (2009), Forced and internal twentieth-century SST trends in the North Atlantic, *J. Clim*, *22*, 1469–1481, doi:10.1175/2008JCLI2561.1.

Wang, S., J. Huang, Y. He, and Y. Guan (2014), Combined effects of the Pacific Decadal Oscillation and El Niño–Southern Oscillation on global land dry-wet changes, *Sci. Rep.*, *4*, 6651, doi:10.1038/srep06651.

Ward, M. N. (1998), Diagnosis and short-lead time prediction of summer rainfall in Tropical North Africa at interannual and multidecadal time scales, *J. Clim.*, *11*, 3167–3191.

Wentz, F. J., L. Ricciardulli, K. Hilburn, and C. Mears (2007), How much more rain will global warming bring?, *Science*, *317*, 233–235.

Xie, P., and P. A. Arkin (1997), Global precipitation: A 17 year monthly analysis based on gauge observations, satellite estimates, and numerical model outputs, *Bull. Am. Meteorol. Soc.*, *78*, 2539–2558.

10.1002/2014GL062451

Yoon, J. H., and N. Zeng (2010), An Atlantic influence on Amazon rainfall, *Clim. Dyn.*, *34*(2–3), 249–264, doi:10.1007/s00382-009-0551-6.

Zeng, N., J. H. Yoon, J. A. Marengo, A. Subramaniam, C. A. Nobre, A. Mariotti, and J. D. Neelin (2008), Causes and impacts of the 2005 Amazon drought, *Environ. Res. Lett.*, *3*, 014002, doi:10.1088/1748-9326/3/1/014002.

Zhang, R., and T. L. Delworth (2006), Impact of Atlantic multidecadal oscillations on India/Sahel rainfall and Atlantic hurricanes, *Geophys. Res. Lett.*, *33*, L17712, doi:10.1029/2006GL026267.